Article:
Lu, X, Nečas, D, Meng, Q orcid.org/0000-0002-6708-5585 et al. (4 more authors) (2020) Towards the direct validation of computational lubrication modelling of hip replacements. Tribology International, 146. 106240. p. 106240. ISSN 0301-679X

https://doi.org/10.1016/j.triboint.2020.106240

Submit to Tribology International as a research paper (R1)

Towards the Direct Validation of Computational Lubrication Modelling of Hip Replacements

Xianjiu Lu[a,b], David Nečas[b], Qingen Meng[c,*1], David Rebenda[b], Martin Vrbka[b], Martin Hartl[b], Zhongmin Jin[a,c,d,*2]

[a] State Key Laboratory for Manufacturing Systems Engineering, Xi'an Jiaotong University, 710054, Xi'an, Shanxi, China

[b] Institute of Machine and Industrial Design, Faculty of Mechanical Engineering, Brno University of Technology, Technická 2896/2, 616 69 Brno, Czech Republic

[c] School of Mechanical Engineering, University of Leeds, LS2 9JT, UK

[d] Tribology Research Institute, School of Mechanical Engineering, Southwest Jiaotong University, Chengdu, 610031, Sichuan, China

*1 Corresponding author:
Tel: 44 113 343 9740
Fax: 44 113 242 4611
Email: Q.Meng@leeds.ac.uk

*2 Corresponding author:
Tel: 0086-13689289660
Email: zmjin@mail.xjtu.edu.cn

Abstract: This study attempted to provide insights into validating computational lubrication modelling of hip replacements. Direct comparisons between experimental measurements and numerical simulations were conducted for the central film thickness in a CoCr-on-glass hip bearing pair. A low-viscosity mineral oil and a 25% bovine serum were used as lubricants, respectively. Results indicated that for the low-viscosity lubricant case, the film thicknesses predicted by the computational model were comparable to the experimental measurements. For the bovine serum case, the computational results did not agree with those measured by experiments due to the viscosity model adopted in the computational models. A new effective viscosity equation was proposed to accurately predict the lubrication performance of hip replacements for protein-containing lubricants under transient conditions.

Keywords: artificial hip joint; lubrication; computational modelling; validation

1 Introduction

Hip replacements have been considered as one of the most successful surgical treatments of hip joint diseases, such as osteoarthritis, rheumatoid arthritis, and osteonecrosis [1]. The wear particles produced in hip replacements are a potential risk of adverse biological reactions [2]. An effective lubricant film can prevent the bearing surfaces from the direct asperity contact and significantly minimize the amount of wear debris. Therefore, understanding the lubrication performance of hip replacements is extremely important. Because the *in-vivo* measurement of the lubricant film thickness in hip replacements is very difficult (if not impossible) to achieve at present, computational modelling has played a significant role in investigating the lubrication performance of hip replacements.

Indeed, computational lubrication modelling has provided important information for the design and adoption of hip replacements. For instance, Dowson et al. [3] pointed out that metal-on-metal hip replacements operate in the mixed-lubrication regime and ceramic-on-ceramic hip replacements are more likely to achieve full fluid film lubrication due to their smooth bearing surfaces. Jin et al. [4-8] found that a smaller clearance and a larger size are beneficial for the lubrication performance of hip replacements. Furthermore, Liu et al. [8] and Meng et al. [9] found that the underneath soft structure of hip replacements and aspherical bearing surfaces are helpful for improving the lubrication performance, respectively.

The full numerical solutions mentioned above have been well verified by mesh convergence studies [10] and comparing with dry contact mechanics analyses [5, 9, 10]. Moreover, some of the conclusions were indirectly validated by wear test results. For instance, Dowson et al. [11] confirmed that larger head diameters and smaller clearances produced lower wear rate, which indirectly validated the previous theoretical lubrication analyses [4-8]. The direct comparison of the lubrication performance of hip replacements under the same operating conditions between computational modelling and experiments can provide confidence for both approaches. For instance, such a comparison can validate the governing equations and related assumptions of the computational model and provide more reliable theoretical supports for experiments. However, due to the difficulties in the full numerical solution and the experimental tests of the lubrication performance of hip replacements, no direct comparison between the full numerical models and the experiments under

the same operating conditions has been conducted for the lubrication performance of hip replacements.

Experimental techniques to measure the lubricant film thickness of hip replacements have been substantially developed in the last decade. Notably, the optical interferometry method has been employed to study the lubricant film thickness of artificial hip joints [12-19]. The early-stage studies investigated the effects of protein-solution lubricants on the film thickness of hip replacements with the optical interferometry method, employing a non-conformal ball-on-disc configuration to represent the conformal contact between the femoral head and the acetabular cup of hip replacements [14-17, 20, 21]. Recently, Vrbka et al. [22] developed the experimental technique to measure the lubricant film thickness between a CoCr head and a glass cup, which made measuring the film thickness of hip replacements with the realistic geometric representation feasible. Based on this optical interferometry technique, the effects of lubricant constituents, diameter, clearance and materials on the lubricant film formation of hip replacements were examined [23, 24]. This experimental technique has made the validation of the computational lubrication models of hip replacements possible, especially when the realistic conditions of hip replacements (e.g., geometry, loading and motion, and rheology of lubricants) are all taken into consideration.

Therefore, this paper intended to provide insights into the direct validation of the current full numerical lubrication model by directly comparing it with experimental measurements. For this purpose, the lubrication film thicknesses between a CoCr femoral head and a glass acetabular cup, lubricated by a low-viscosity mineral oil and a bovine serum solution, respectively, were numerically solved using a computational lubrication model and experimentally measured using the optical interferometry method.

2 Materials and methods

2.1 Materials

The lubricated contact between a CoCr femoral head and a glass acetabular cup was studied in this study. Glass acetabular cups are not used in modern realistic hip replacements. The reason for using a glass acetabular cup was that the optical interferometry method, in which the acetabular cup has to be transparent to observe

the film formation inside the contact, was employed to measure the film thickness. The radius of the femoral head was 13.985 mm and the radial clearance between the cup and the head was 40 μm. The outside radius of the cup was 24.025 mm, resulting in a cup thickness of 10 mm. The maximum pressure that the contact surfaces of the CoCr head and glass acetabular cup were subjected to in this study was about 30 MPa, which was much smaller than the yielding stresses of the CoCr alloy and the compressive strength of glass. Therefore, both the CoCr head and glass acetabular cup were assumed linear elastic. The material properties and geometry of the metallic head and THE glass cup are summarized in Table 1.

Two types of lubricants were used in this study. First, a low-viscosity mineral oil (SN100) was adopted to exclude the protein aggregation and adsorption effects in synovial fluids and the bovine serum solution. The second type lubricant was a 25% bovine serum solution. This lubricant was chosen because the bovine serum solution is widely used in wear and lubrication experiments to represent the synovial fluid [20, 25].

2.2 Loading and motion conditions

The configuration of the pendulum hip joint simulator (Figure 1) was considered in the present study. The outer surface of the cup was fixed. The head was positioned at the centre of the cup with an applied vertical load of 532 N. The head rotated around the z-axis in Figure 1 with an angular speed of ω_z to simulate the flexion-extension motion of the hip joint.

Two types of motions were adopted as the inputs of the lubrication systems of this study. The analogous sinusoidal angular velocity shown in Figure 2a was used for the SN 100 oil case. The maximum amplitude of the oscillation was around 1 rad/s, with a frequency of 0.5 Hz. The start-up and shut-down processes of the pendulum were both considered in the numerical analyses and experiments (Figure 2a). To compare the computational results with the published experimental results [22], the amplitude-decayed sinusoidal angular velocities (Figure 2b) were adopted for the 25% bovine serum case. In this case, the amplitude of the maximum angular velocity decayed from 0.45 rad/s to zero, with a frequency of 0.5 Hz (Figure 2b).

2.3 Computational methods

2.3.1 Viscous properties of the lubricants

The viscosities of the mineral oil (SN100) under different pressures (varying from 0.0 to 40.1 MPa) were measured at 25℃. The measured viscosity values were subsequently curve-fitted to the Roelands' viscosity-pressure equation [26]

$$\eta = \eta_0 \exp\left\{\left(\ln \eta_0 + 9.67\right)\left[\left(1 + 5.1 \times 10^{-9} p\right)^z - 1\right]\right\} \quad (1)$$

The fitted values for η_0 and z were 0.033 Pa·s and 0.703, respectively. The error in the viscosity between the values obtained from the fitted relation and the measured values was 0.35%.

To provide more insights into the direct validation of the computational lubrication models of hip replacements, two types of viscous models were used for the 25% bovine serum. As demonstrated in the previous studies [20, 27], the viscosity of the 25% bovine serum solution is constant when the shear rate is above 1000 s^{-1}. The shear rates in most of the contact area of the hip replacement are above 1000 s^{-1}, and the lower shear rates only exist at the boundaries of the contact area, which have little influence on the overall film thickness distribution. Therefore, it was a common and reasonable method to adopt a constant viscosity value (0.0009 ~ 0.0025 Pa·s) for the 25% bovine serum in the computational lubrication studies of hip replacements [8, 11, 28]. This study examined this constant-viscosity model by adopting a value of 0.002 Pa·s for the 25% bovine serum solution.

Moreover, Myant et al. [15] found that under steady-state conditions, the boundary layer formed on the surfaces was augmented by the high viscosity fluid film generated by the hydrodynamic effect. The lubricant film thickness was thicker for low-speed cases, and an effective velocity-viscosity relation was proposed for the bovine serum to consider the protein aggregation effect. Therefore, this velocity-viscosity relation (equation (2)) [15] was also used to model the viscosity of the bovine serum solution in the numerical lubrication model.

$$\eta = k_1 U^{z_1} \quad (2)$$

where U is the entrainment speed, and the values of the coefficients (k_1 = 3.422 and z_1 = −1.248) were obtained by fitting the viscosity-velocity data presented in literature [15] to equation (2).

2.3.2 Governing equations

The governing equations for a transient computational lubrication model included the Reynolds, the film thickness, the deformation, and the load balance equations. The time-dependent Reynolds equation in spherical coordinates for the ball-in-socket model was [29]

$$\sin\theta\frac{\partial}{\partial\theta}\left(\frac{h^3}{\eta}\sin\theta\frac{\partial p}{\partial\theta}\right)+\frac{\partial}{\partial\varphi}\left(\frac{h^3}{\eta}\frac{\partial p}{\partial\varphi}\right)=6R^2\sin^2\theta\left(\omega(t)\frac{\partial h}{\partial\varphi}+2\frac{\partial h}{\partial t}\right) \tag{3}$$

where p is the hydrodynamic pressure; h is the film thickness; η is the viscosity of the lubricants, which was described in section 2.3.1 for the mineral oil and bovine serum cases; t is time; ω is the angular velocity of the femoral head; and ϕ and θ are the spherical coordinates. The boundary conditions of the Reynolds equation at each time instant were

$$p(0,\theta)=p(\pi,\theta)=p(\varphi,0)=p(\varphi,\pi)=0$$

$$\partial p/\partial\varphi=\partial p/\partial\theta=0,\quad 0<\varphi<\pi,\quad 0<\theta<\pi$$

The cavitation boundary condition was achieved by setting the obtained negative pressure as zero during the relaxation process in the entire calculation domain.

The film thickness equation contained both the undeformed gap between the spherical bearing surfaces of hip replacements and the elastic deformation of the bearing surfaces due to the hydrodynamic pressure [30]

$$h(\varphi,\theta)=c-e_x\sin\theta\cos\varphi-e_y\sin\theta\sin\varphi+\delta(\varphi,\theta) \tag{4}$$

where c represents the radial clearance between the cup and the head; e_x and e_y are the eccentricity components of the centre of the head with respect to the cup in the ϕ and θ direction, respectively. $\delta(\phi, \theta)$ is the elastic deformation of the bearing surfaces.

The external load components were balanced by the integration of the hydrodynamic pressure [30]

$$\begin{aligned} f_x&=R_C^2\int_0^\pi\int_0^\pi p\sin^2\theta\cos\varphi d\theta d\varphi=0\\ f_y&=R_C^2\int_0^\pi\int_0^\pi p\sin^2\theta\sin\varphi d\theta d\varphi=W_y\\ f_z&=R_C^2\int_0^\pi\int_0^\pi p\sin\theta\cos\theta d\theta d\varphi=0 \end{aligned} \tag{5}$$

2.3.3 Numerical methods

To facilitate the calculation process and improve the stability of numerical analysis, all the governing equations were non-dimensionalised [31]. Each oscillating cycle was divided into 50 instants. At each instant, the Reynolds equation was solved using a multi-grid technique [31] and the deformation was calculated using a Fast Fourier Transform method [32]. Three levels of grids were adopted for the multi-grid method. On different levels, the calculation domains of the spherical hip bearing surfaces (from 0 to π for both ϕ and θ) were discretised into different numbers of nodes. The number of nodes on the finest level was 257 in both the ϕ and θ directions [28]. The load balance equation was solved by iteratively adjusting the eccentricities in the ϕ and θ direction according to the difference between the integration of the hydrodynamic pressure and the applied load [31]. To be consistent with the experiments, at the first time instant (when $t = 0$), the head and the cup were assumed in contact and the pressure was set as zero. Then these film thicknesses and pressure values were used as the initial values for the next time instant.

At each instant of the transient lubrication analysis, the deformation was calculated using the following equation [30]

$$\delta_{i,j} = \sum_k \sum_l C_{i,j,k,l} p_{k,l} \tag{6}$$

where $C_{i,j,k,l}$ is the displacement coefficients matrix, defined by the average displacement at node (i, j) caused by a unit pressure distribution at node (k, l). The displacement coefficients were calculated using the method developed by Wang and Jin [32]. Finite element models were constructed for the head and cup first. Then a unit pressure was applied to the element at the centre of the articulating surface of the head and the cup, respectively. The normal elastic deformations of the head and the cup along a longitudinal line were obtained through finite element analyses. These displacements were used to curve fit a displacement influence function of the spherical distance. Finally, the deformation coefficients were calculated for all the nodes on the articulating surfaces of the head and the cup using the fitted function.

Because three levels of grids were used for the multi-grid method, the deformation coefficients were calculated for different numbers of nodes (i.e., 65×65，129×129，and 257×257). The accuracy of the elastic deformation coefficients was examined by calculating the deformation caused by a given pressure distribution (using equation (6)) and then comparing it with the deformation obtained from a finite element

analysis. To achieve this, a parabolic pressure distribution with the maximum pressure of 10 MPa and a half contact angle of 30 degrees was applied to the central region of the bearing surface of the cup and head [32]. In this study, the largest oscillating angle of the pendulum was 32 degrees and the contact between the head and the cup was within the central region of the cup (i.e., not close to the rim of the cup). Therefore, the position of the parabolic pressure distribution would not affect the calculated deformation [32].

2.4 Experiment methods

The pendulum hip joint simulator and the optical imaging system [22, 24, 33, 34] were employed to measure the film thickness of the hip replacement. In the pendulum hip simulator, the glass acetabular cup was fixed in a base frame and the femoral head was connected to a swinging pendulum by a pendulum arm. The swinging motion of the pendulum was in the flexion-extension plane because the major velocity component of hip implants is in the flexion/extension direction [22]. The pendulum was driven manually, allowing a continuous motion in the flexion-extension plane. The thin film colorimetric interferometry method [33] was employed to evaluate the film thickness. The resolution of this technique could reach 1 nm [33]. The maximum detectable film thickness is around 900 nm. The contact was captured by a complementary metal-oxide-semiconductor (CMOS) high-speed camera (Phantom V710). The details of the test devices and measurement method can be found in the literature [22, 24, 34]. In general, three basic steps were involved. First, the calibration curves, which gave the relationship between the colors of the interferograms and the values of the film thickness, was obtained based on a lightly loaded static contact. Second, using the high-speed camera, the interferograms of the lubricant film were captured for the load and motion conditions in Section 2.2. Finally, the film thickness within the contact area was evaluated by comparing the captured interferograms with the calibrated curves.

The contact area continuously changed within the cup over the oscillation. However, only the central film thickness when the pendulum arm reached the vertical (equilibrium) position was measured because the high-speed camera was fixed underneath the central contact position of the cup. At each instant, the measured central film thickness was the average value of the film thicknesses within a circular area of 40 pixels (diameter of around 0.2 mm) [24]. When the cross-sectional central

film thicknesses in the entraining and side leakage directions were compared with the numerical solutions, the film thickness values along one pixel in the side leakage or entraining direction and 421 pixels in the perpendicular direction were extracted from the interferograms.

2.5 A new entrainment velocity-effective viscosity relation

Based on the assumption that the iso-viscous viscosity and the effective viscosity model (equation (2)) could not produce accurate film thicknesses for the bovine serum case, a new entrainment velocity-effective viscosity relation was proposed. The experimentally measured central film thicknesses [22] were used as the target values in a numerical fitting process. At each instant, an initial viscosity was given to the model and the governing equations were solved using the given viscosity. Then the obtained central film thickness was compared with the target values. The viscosity was subsequently updated based on the difference in the central film thickness until the relative difference between the numerical and experimental values was less than a given criterion (10^{-3}). After the effective viscosity values were obtained for each instant of the first three seconds of the amplitude-decayed sinusoidal oscillation, the effective viscosities were curve fitted to equation (7) to obtain the relationship between the effective viscosity and the entrainment velocity (Figure 8).

$$\eta = \eta_\infty + \frac{\eta_0 - \eta_\infty}{1 + \left(u / c\right)^{p_1}} \tag{7}$$

where η_0 is the effective viscosity when the entrainment speed is zero; η_∞ is the effective viscosity when the entrainment speed is infinity; u is the entrainment speed; c and p_1 are curve fitted constants. This equation was close to the Cross rheological model [35], which describes the relationship between the shear rate and viscosity. The Cross rheological model has been used in the previous study [20] to represent the bovine serum solution and showed good consistency. Enlightened by these previous studies, the relationship between the effective viscosity and the entrainment velocity (equation (7)) followed a similar form. However, for the convenience of the application in numerical analyses, the shear rate in the Cross rheological model was replaced by the entrainment velocity.

After the parameters in equation (7) were obtained from the fitting process, the fitted entrainment velocity-effective viscosity relation was used to solve the governing

equations in the numerical analyses for the whole oscillation process (48 s) and the results were compared with the experiments. Since only the effective viscosities of the first 3 seconds of the amplitude-decayed sinusoidal oscillation were used when the constants of equation (7) were derived, the comparison of the film thickness at other instants (from 3 s to 48 s) between the numerical analyses and the experimental measurements can validate the proposed new entrainment velocity-effective viscosity relation.

3 Results

Accurate elastic deformation of the CoCr head and the glass cup was predicted from the displacement coefficients matrix (Figure 4). The deformations of the CoCr head and the glass cup calculated from the deformation coefficients was very close to those solved from the FEA (Figure 4). The differences in the predicted deformation between the deformation coefficients and the FEA were less than 1.5%.

For the SN100 oil case, the central film thickness at the vertical position of the pendulum arm predicted by the computational model agreed well with the average central film thickness measured by the experiment (Figure 5). When the oscillation was relatively steady (after 6.0 seconds), the central film thickness in the equilibrium position predicted by the numerical simulation was around 250 nm and the value measured by the experiment was about 260 nm. Moreover, after the oscillation was steady, the predicted maximum pressure oscillated around 27.5 MPa with a small amplitude of 2.5 MPa. To compare, the maximum Hertz pressure of the system was 26.5 MPa. Moreover, during the oscillation, the maximum angular velocities and the maximum central film thicknesses of the numerical simulation and experiment did not occur at the same the instants (Figure 5). The cross-sectional film profiles in the entraining direction and the side leakage direction predicted by the numerical solutions were very close to those measured by the experiments, although the experimentally measured cross-sectional film thickness fluctuated at all the three instants investigated in this study (Figure 6). The maximum fluctuation amplitude of the experimentally measured film thickness was around 50 nm (Figure 6).

The central film thicknesses predicted by the iso-viscous model and the effective viscosity model did not agree well with the experimental measurements (Figure 7). The variation in the central film thickness predicted by the iso-viscous model

decreased during the first a few seconds and reached a constant value. This trend was quite similar to the experimental measurements. However, the steady central film thickness predicted by the iso-viscous model was approximately five times smaller than the experimental measurements. The effective viscosity model proposed in reference [15] predicted a gradually decreasing trend for the central film thickness. However, during the whole cycle of the oscillation, the effective viscosity significantly overestimated the central film thickness (more than the double of the experimental measurement, Figure 7).

The following values were obtained for the variables of equation (7): $\eta_\infty = 0.038$ Pa·s, $\eta_0 = 0.352$ Pa·s, $c = 0.175$ mm/s and $p_1 = 1.668$ (Figure 8). Compared with the original viscosities derived from the experiments, the residual sum of squares of the fitted entrainment velocity-effective viscosity relation was 0.017. Even if only the effective viscosities of the first three seconds of the amplitude-decayed sinusoidal oscillation were used to derive the constants of equation (7), the central film thickness calculated using the new entrainment velocity-effective viscosity equation agreed very well with the experimental measurements during the whole oscillation process (Figure 9). For the period from 3 s to 48 s, the average relative error in the central film thicknesses calculated from the new entrainment velocity-effective viscosity equation was about 14%.

To provide more insights into the lubrication mechanism of hip replacements, the central film thicknesses and shear rates of an oscillation cycle produced by the three viscosity models (i.e., the iso-viscous, the effective viscosity model proposed by Myant et al., and the effective viscosity model proposed in this study) were plotted against the velocity in Figure 10 (a). Generally, apart from a few instants when the entraining velocity was nearly zero, the shear rates calculated from the three viscosity models were all greater than 10^3 s^{-1} during the whole cycle. Moreover, because the film thickness only varied very slightly during one cycle, the variations of the shear rates of the three viscosity models were all determined by that of the velocity (Figure 10 (a)). The variations in the entraining velocity, the shear rate, and the effective viscosity within one cycle were investigated for the effective viscosity models proposed by Myant et al. and this study (Figure 10 (b) and (c), respectively). Clearly, the shear rates produced by these two effective viscosity models were at the same order of magnitude. However, the effective viscosities of Myant et al.'s model

(equation (2)) varied from 1.07 Pa·s to an extremely large value (theoretically, infinity), while those of the new viscosity model proposed in this study varied from 0.10 to 0.35 Pa·s.

4 Discussion

Understanding the lubrication performance of hip replacements is very important because an effective lubricant film can prevent the bearing surfaces from the direct asperity contact and significantly minimize the amount of wear debris. The *in vivo* measurement of the lubricant film thickness of hip replacements is still very difficult. Therefore, computational modelling has played a significant role in investigating the lubrication performance of hip replacements. Previous full numerical solutions for the lubrication performance of hip replacements have been well verified by mesh convergence studies [10] and comparing with dry contact mechanics analyses [5, 9, 10], and indirectly validated by wear test results [11]. However, due to the difficulties in the full numerical solution and experimental measurements of the film thickness of hip replacements, the direct validation of the full numerical computational model has not been conducted, especially when considering the realistic ball-in-socket geometry of the hip replacements. A validated computational model can provide more reliable results, which may be difficult or even impossible to obtain from the direct experimental observation. Therefore, this study intended to compare the lubricant film thickness of a CoCr-glass replacement calculated from full numerical analyses with that measured by experiments, thus providing insights into the direct validation of current computational lubrication models for hip replacements.

At first, a low-viscosity mineral oil SN 100 (η_0 = 0.0332 Pa·s) was adopted to exclude the protein aggregation effect in synovial fluids and bovine serum solutions [14-17, 21]. The satisfactory agreement between the computational and experimental averaged central film thickness (Figure 5) indicated that for the given ball-in-socket configuration of hip replacements, the computational lubrication model could accurately predict the averaged central film thickness. Moreover, the agreement in the cross-sectional film profiles in the entraining and side leakage directions between the experiments and numerical analyses (Figure 6) also supported the above statement. The disagreement in the positions of the maximum angular velocities and the maximum central film thicknesses of the numerical simulation and experiment was

due to the well-known time lag caused by the squeeze-film action [10, 36].

The small disagreements between the experiments and the numerical simulation in the cross-sectional film profiles of the low-viscosity lubricant case (Figure 6) were mainly due to the effects of the surface roughness and the slightly different input conditions. When the transient central film thicknesses were measured, the average values of the film thicknesses within a 0.2 mm diameter circular area (Figure 5) were adopted. Therefore, the positive and negative effects of the roughness were cancelled out and the experimentally measured average central film thicknesses were close to those of the numerical analysis. When the cross-sectional film profiles in the entraining (or the side leakage) direction were plotted, the values along one pixel in the entraining (or the side leakage) direction and 421 pixels in the perpendicular direction were extracted from the interferograms. Therefore, the differences between the experiments and the numerical simulation became obvious for the cross-sectional film profiles (Figure 6). The effect of the surface roughness can be clearly seen from the fluctuation of the experimentally measured cross-sectional film profiles. However, the surface roughness was not considered in the computational model due to excessively expensive computational costs to capture the surface roughness in the numerical simulation. Moreover, to achieve the analogous sinusoidal angular velocity (Figure 2a), the pendulum was driven with slight manual assistance, which might introduce a slight impact on the input velocity and affect the accuracy of the measurement of the film thickness.

If the effect of the protein aggregation is not considered, both the bovine serum and synovial fluid are iso-viscous lubricants with very low viscosities [20, 27] when the shear rate is greater than 1000 s^{-1}. The previous computational lubrication models have adopted such viscous properties for the bovine serum and synovial fluid [8, 11, 28, 29, 31, 37]. Therefore, based on the above discussion for the low-viscosity mineral oil case, it is reasonable to believe that these numerical studies were accurate. However, in the study using the bovine serum solution as the lubricant, the film thicknesses predicted by the iso-viscous model were approximately five times smaller than the experimental measurements (Figure 7), although the shear rates in the hip replacement were indeed larger than 1000 s^{-1} apart from a few time instants when the angular velocity tended to be zero (Figure 10 (a)).

The disagreement in the film thickness between the experimental measurements and

the theoretical lubrication analyses has been reported for the protein-containing lubricants, such as the bovine serum solutions [15]. A gel-like protein phase was found to form at the inlet of the lubricated contact area due to the aggregation of protein molecules [15]. At low speeds, when the gel-like protein phase was entrained into the contact, a high-viscosity film was formed. As the speed increased, the gel appeared to shear thin, producing much lower lubricant film thickness [15]. To consider this protein aggregation effect of the bovine serum solution, Myant et al. [15] proposed a relation between the effective viscosity and the entraining velocity ($\eta = k_1 U^{z_1}$) based on the Hooke's central film thickness equation and the measured central film thickness. However, in this study, this effective viscosity model did not accurately predict the central film thickness for the bovine serum solution case (Figure 7). Several reasons may have contributed to the disagreement. First, the amplitude-decayed sinusoidal angular velocities reduced from 0.45 rad/s to 0 rad/s. Therefore, the corresponding entrainment velocities were 3.1 mm/s to zero. The equivalent viscosity would approach infinity when the entrainment velocity is zero if equation (2) is used to represent the viscosity (Figure 10 (b)). This is not physically reasonable. Secondly, Hooke's central film thickness equation is only applicable for steady-state problems. Therefore, the transient effect caused by the oscillation of the pendulum was not considered in equation (2). In addition, a ball-in-socket configuration was modelled in this study, while a ball-on-disc test device was used in Myant et al.'s experiments [15]. The protein aggregation effect of the bovine serum or synovial fluid may play a different role in the ball-on-disc contact from that of the ball-in-socket contact. Therefore, the effective viscosity fitted from the ball-on-disc experiments may not be suitable for the lubrication simulation of hip replacements with a ball-in-socket geometry.

The newly proposed relation (equation (7)) between the viscosity and the entraining velocity followed the form of the Cross rheological model [35] but replaced the shear rate in the Cross rheological model using the entrainment velocity. Since the film thickness changed very slightly in one cycle and the variation of the shear rate was consistent with the velocity (Figures 10 (a) and (c)), equation (7) was essentially similar to the Cross rheological model. Moreover, the effective viscosities calculated by equation (7) were higher for the lower entrainment velocities and lower for the higher lower entrainment velocities (Figures 10 (c)). Thus, the protein aggregation

effect described above was well represented by this new effective viscosity equation. Moreover, because the values of the parameters of equation (7) were derived from the full numerical solutions considering the transient effect and the realistic ball-in-socket geometry of hip replacements, these factors were also incorporated into the effective viscosity. Therefore, it is reasonable to believe that for bovine serum solution lubricants, this new effective viscosity equation can predict the transient lubrication film thickness of hip replacements more accurately.

Indeed, the central film thicknesses calculated using the new effective viscosity equation were much closer to the experimental measurements than those produced by the iso-viscous model and Myant et al.'s effective viscosity model (Figures 7 and 9). Because only the effective viscosities of the first three seconds of the oscillation were used when the parameters in equation (7) were derived, the good agreement in the film thickness at the rest of time instants (from 3 s to 48 s) between the numerical analyses and the experimental measurements could be considered as the validation of the new effective viscosity equation. Moreover, the small difference (14%) between the numerical analyses and the experimental measurements could be improved by using more time instants to derive the parameters in equation (7).

Although the new effective viscosity equation was able to represent the higher viscosity lubricant caused by the gel-like protein phase, the real properties of the bovine serum and synovial fluid solution are more complicated than just a higher viscosity value. They usually tend to exhibit complex time-dependent film thickness behaviour [15], which is due to the particular properties of the bovine serum and synovial fluids solutions, such as viscoelasticity. In addition to the fluid film lubrication, a deposition of boundary film may also be formed on the contact surfaces of the hip replacements [38]. This boundary film appears to be nonhomogeneous and chaotic due to the complex multi-mode regimes of protein suspensions during sliding. Moreover, it has been observed that the gel-phase shows periodic characteristics when entrained into the contact area. The formed thick protein layer could be easily removed or disturbed by the scratches on the implant surface [15]. In addition to proteins, the bovine serum and synovial fluids also contain other compositions such as hyaluronic acid and phospholipids [21, 39]. Therefore, although a new effective viscosity equation was proposed in this study, it is still an approximate description of the rheology of the bovine serum and synovial fluid solutions. To more accurately

simulate the lubrication process of hip replacements, more sophisticated rheology models need to be developed to consider the above factors in future studies.

5 Conclusions

To validate the present full numerical lubrication models of hip replacements, the film thicknesses within the contact of a CoCr femoral head and a glass acetabular cup were numerically predicted by a computational model and experimentally measured by the optical interferometry method. A low-viscosity mineral-oil lubricant and a 25% bovine serum were used as the lubricants, respectively. Direct comparisons between the experimental measurements and numerical simulations were conducted for the film thickness. The main findings included:

- The current full numerical analyses for hip replacements could predict relatively accurate film thickness for the low-viscosity lubricant without macromolecular substances contained.
- The film thickness was not accurately predicted when both the iso-viscous model and the effective viscosity equation proposed by Myant et al. were used for the bovine serum solution.
- An new effective viscosity equation, incorporating the realistic geometry of hip replacements, transient effects, and the protein aggregation behaviour, was proposed for the bovine serum solution.

Conflicts of interest statement

There is no conflict of interest.

Acknowledgements

This study was carried out under the project LTAUSA17150 with financial support from the Ministry of Education, Youth and Sports of the Czech Republic. The research was also supported by National Natural Science Foundation of China [grant number 51323007].

References

[1] Mattei L, Di Puccio F, et al. Lubrication and wear modelling of artificial hip joints: A review. Tribology International. 2011;44:532-49.

[2] Liu F, Jin ZM, et al. Transient elastohydrodynamic lubrication analysis of a metal-on-metal hip implant under simulator-tested conditions. Proceedings CDROM of the Sixth World Congress on Computational Mechanics in Conjunction with the Second Asian-Pacific Congress on Computational Mechanics, Beijing. 2004.

[3] Dowson D. Elastohydrodynamic lubrication in 'soft-on-soft' natural synovial joints; 'hard-on-soft' cushion and 'hard-on-hard' metal-on-metal total joint replacements. Springer Netherlands. 2006:297-308.

[4] Jin ZM, Dowson D, et al. Analysis of fluid film lubrication in artificial hip joint replacements with surfaces of high elastic modulus. Proceedings of the Institution of Mechanical Engineers, Part H: Journal of Engineering in Medicine. 1997;211:247-56.

[5] Meng QE, Liu F, et al. Contact mechanics and lubrication analyses of ceramic-on-metal total hip replacements. Tribology International. 2013;63:51-60.

[6] Liu F, Jin ZM, et al. Importance of head diameter, clearance, and cup wall thickness in elastohydrodynamic lubrication analysis of metal-on-metal hip resurfacing prostheses. Proceedings of the Institution of Mechanical Engineers Part H, Journal of engineering in medicine. 2006;220:695-704.

[7] Jalali-Vahid D, Jagatia M, et al. Prediction of lubricating film thickness in a ball-in-socket model with a soft lining representing human natural and artificial hip joints. Proceedings of the Institution of Mechanical Engineers, Part J: Journal of Engineering Tribology. 2001;215:363-72.

[8] Liu F, Wang, FC, et al. Steady-state elastohydrodynamic lubrication analysis of a metal-on-metal hip implant employing a metallic cup with an ultra-high molecular weight polyethylene backing. Proceedings of the Institution of Mechanical Engineers Part H, Journal of engineering in medicine. 2004;218:261-70.

[9] Meng QE, Gao LM, et al. Contact mechanics and elastohydrodynamic lubrication in a novel metal-on-metal hip implant with an aspherical bearing surface. Journal of biomechanics. 2010;43:849-57.

[10] Meng QE. Elastohydrodynamic Lubrication in Metal-on- Metal Artificial Hip Joints with A Spherical Bearing Surfaces and Complex Structures. PhD thesis, University of Leeds, England. 2010.

[11] Dowson D, Hardaker C, et al. A hip joint simulator study of the performance of metal-on-metal joints. The Journal of Arthroplasty. 2004;19:124-30.

[12] Fan J, Myant CW, Underwood R, Cann PM, Hart A. Inlet protein aggregation: a new mechanism for lubricating film formation with model synovial fluids. Proceedings of the Institution of Mechanical Engineers, Part H: Journal of Engineering in Medicine. 2011;225:696-709.

[13] Mavraki A, Cann PM. Lubricating film thickness measurements with bovine serum. Tribology International. 2011;44:550-6.

[14] Myant C, Underwood R, et al. Lubrication of metal-on-metal hip joints: the effect of protein content and load on film formation and wear. Journal of the

mechanical behavior of biomedical materials. 2012;6:30-40.
[15] Myant C, Cann P. In contact observation of model synovial fluid lubricating mechanisms. Tribology International. 2013;63:97-104.
[16] Myant C, Cann P. On the matter of synovial fluid lubrication: implications for Metal-on-Metal hip tribology. Journal of the mechanical behavior of biomedical materials. 2014;34:338-48.
[17] Myant CW, Cann P, et al. The effect of transient conditions on synovial fluid protein aggregation lubrication. Journal of the mechanical behavior of biomedical materials. 2014;34:349-57.
[18] Vrbka M, Navrat T, et al. Study of film formation in bovine serum lubricated contacts under rolling/sliding conditions. Proceedings of the Institution of Mechanical Engineers, Part J: Journal of Engineering Tribology. 2013;227:459-75.
[19] Vrbka M, Krupka I, et al. In situ measurements of thin films in bovine serum lubricated contacts using optical interferometry. Proceedings of the Institution of Mechanical Engineers Part H, Journal of engineering in medicine. 2014;228:149-58.
[20] Mavraki A, Cann, P. Lubricating film thickness measurements with bovine serum. Tribology International. 2011;44:550-6.
[21] Fan J, Myant C, et al. Inlet protein aggregation: a new mechanism for lubricating film formation with model synovial fluids. Proceedings of the Institution of Mechanical Engineers Part H, Journal of engineering in medicine. 2011;225:696-709.
[22] Vrbka M, Nečas D, et al. Visualization of lubricating films between artificial head and cup with respect to real geometry. Biotribology. 2015;1:61-5.
[23] Nečas D, Vrbka M, et al. The effect of lubricant constituents on lubrication mechanisms in hip joint replacements. Journal of the mechanical behavior of biomedical materials. 2016;55:295-307.
[24] Nečas D, Vrbka M, et al. In situ observation of lubricant film formation in THR considering real conformity: The effect of diameter, clearance and material. Journal of the mechanical behavior of biomedical materials. 2017;69:66-74.
[25] Essner A, Schmidig G, et al. The clinical relevance of hip joint simulator testing: In vitro and in vivo comparisons. Wear. 2005;259:882-6.
[26] Roelands C. Correlational aspects of the viscosity-temperature-pressure relationship of lubricating oils. Doctoral thesis, Technische Hogeschool te Delt. 1966.
[27] Yao JQ, Laurent M, et al. The influences of lubricant and material on polymer/CoCr sliding friction. Wear. 2003;255:780-4.
[28] Liu F, Jin, ZM, et al. Transient elastohydrodynamic lubrication analysis of metal-on-metal hip implant under simulated walking conditions. Journal of biomechanics. 2006;39:905-14.
[29] Jin ZM, Dowson D. A full numerical analysis of hydrodynamic lubrication in artificial hip joint replacements constructed from hard materials. Proceedings of the Institution of Mechanical Engineers, Part C: Journal of Mechanical Engineering Science. 1999;213:355-70.
[30] Jagatia M, Jin ZM. Elastohydrodynamic lubrication analysis of metal-on-metal hip prostheses under steady state entraining motion. Proceedings of the Institution of Mechanical Engineers Part H, Journal of engineering in medicine. 2001;215:531-41.

[31] Meng QE, Gao LM, Liu F, et al. Transient elastohydrodynamic lubrication analysis of a novel metal-on-metal hip prosthesis with an asspherical acetabular bearing surface. Journal of medical biomechanics. 2009;24:352-62.
[32] Wang FC, Jin ZM. Prediction of elastic deformation of acetabular cups and femoral heads for lubrication analysis of artificial hip joints. Proceedings of the Institution of Mechanical Engineers, Part J: Journal of Engineering Tribology. 2004;218:201-9.
[33] Hartl M, Krupka I, et al. Thin Film Colorimetric Interferometry. Tribology Transactions. 2001;44:270-6.
[34] Nečas D, Vrbka M, et al. In situ observation of lubricant film formation in THR considering real conformity: The effect of model synovial fluid composition. Tribology International. 2018;117:206-16.
[35] Cross MM. Rheology of non-Newtonian fluids: a new flow equation for pseudoplastic systems. Journal of colloid science. 1965;20:417-37.
[36] Glovnea RP, Spikes HA. The influence of lubricant properties on EHD film thickness in variable speed conditions. Tribology Series. 2003;43:401-8.
[37] Gao L, Yang P, Dymond I, Fisher J, Jin Z. Effect of surface texturing on the elastohydrodynamic lubrication analysis of metal-on-metal hip implants. Tribology International. 2010;43:1851-60.
[38] Malmsten M. Formulation of absorbed protein layers. Journal of colloid and Interface Science. 1998;20:186-99.
[39] Cooke AF, Dowson D, Wright V. The rheology of synovial fluid and some potential synthetic lubricants for degenerate synovial joints. Engineering in Medicine. 1978;7:66-72.

Table 1: Material and geometrical parameters adopted in this study

Radius of CoCr femoral head, R_H	13.985 mm
Radial clearance, c	40 μm
Thickness of glass cup	10 mm
Elastic modulus of CoCr	230 GPa
Elastic modulus of glass	85 GPa
Poisson's ratio of CoCr	0.3
Poisson's ratio of glass	0.209

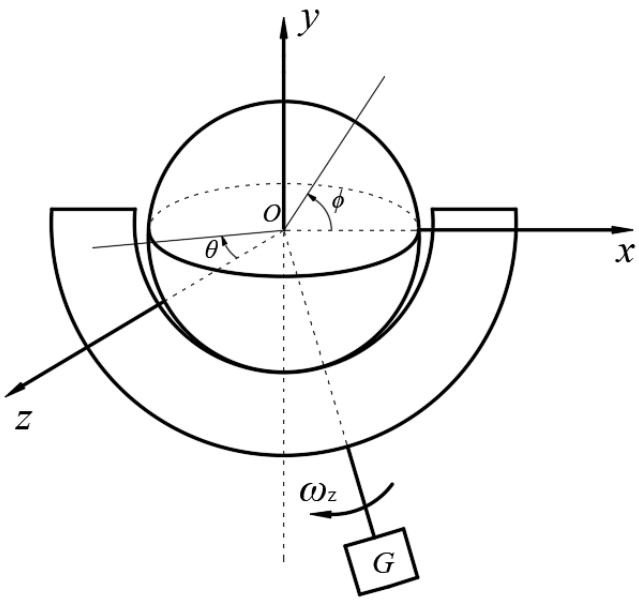

Figure 1 A ball-in-socket lubrication model of the pendulum hip joint simulator.

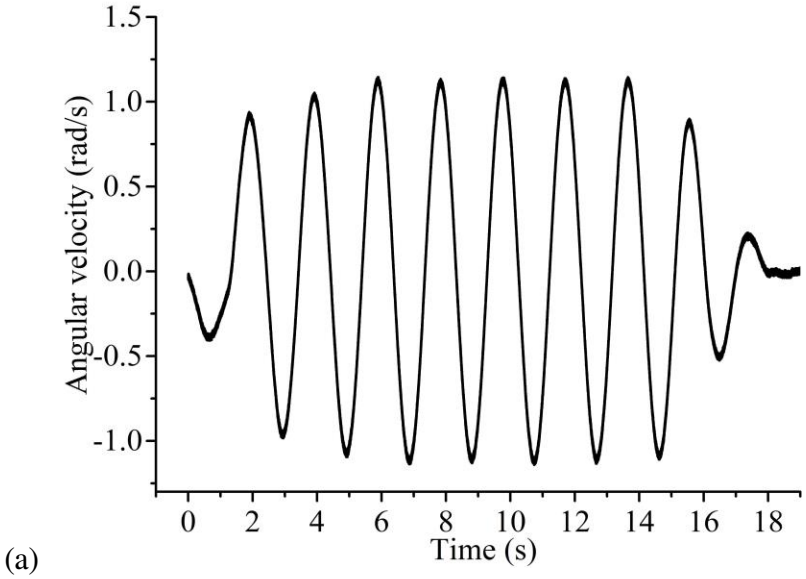

(a)

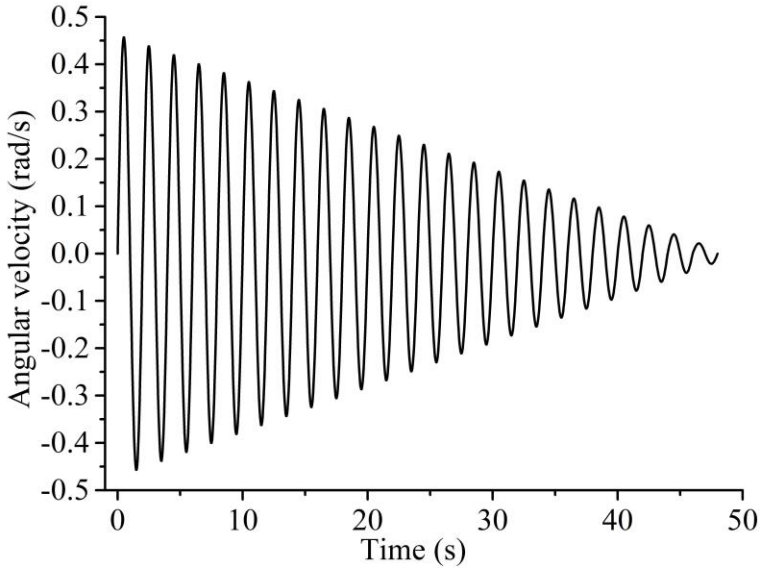

(b)

Figure 2 (a) The analogous sinusoidal angular velocity used for the SN 100 oil case (b) The amplitude-decayed sinusoidal angular velocities adopted for the 25% bovine serum case.

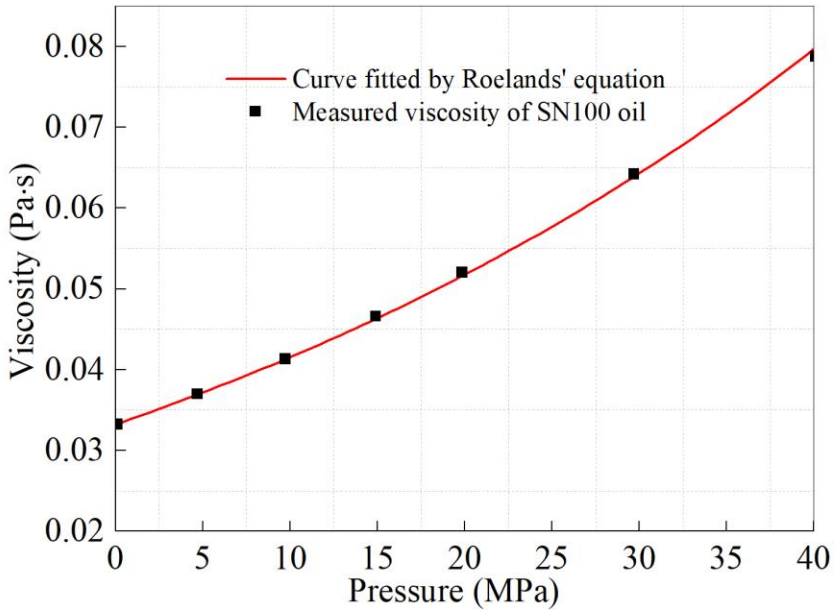

(a)

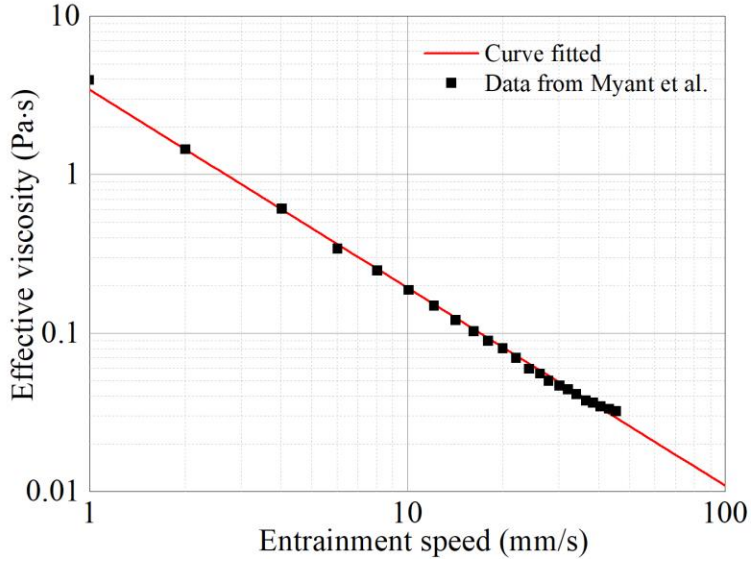

(b)

Figure 3 (a) The measured and curve-fitted Roelands' viscosity-pressure relationship for the SN100 oil (b) The entrainment velocity-effective viscosity relation proposed by Myant et al. [15] for the 25% bovine serum solution.

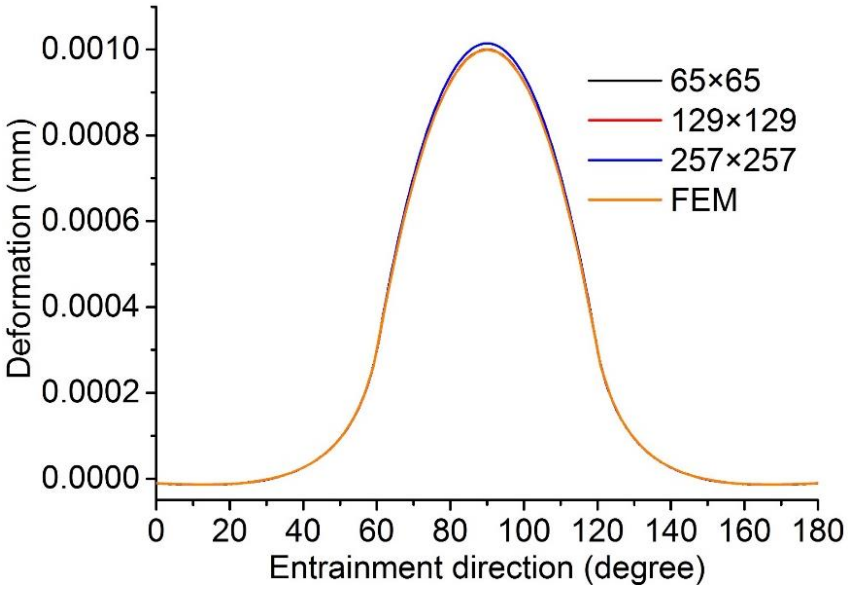

Figure 4 The elastic deformation of the CoCr head and the glass acetabular cup in the latitude direction caused by a parabolic pressure distribution, calculated from the elastic deformation coefficients of the three levels of grid and the finite element method.

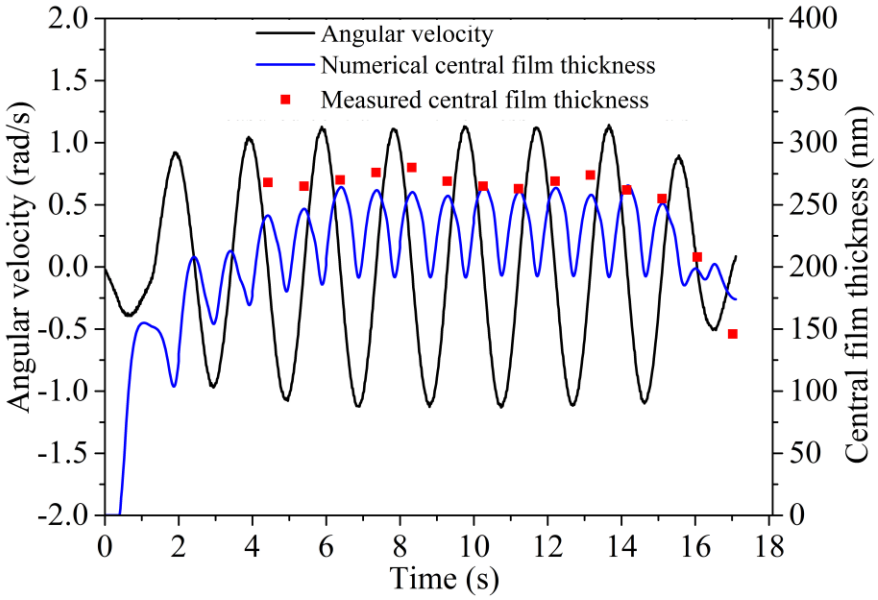

Figure 5 The comparison of the central film thickness between the experimental measurements and the numerical analyses for the low-viscosity mineral oil case (SN100, $\eta_0 = 0.0332$ Pa·s).

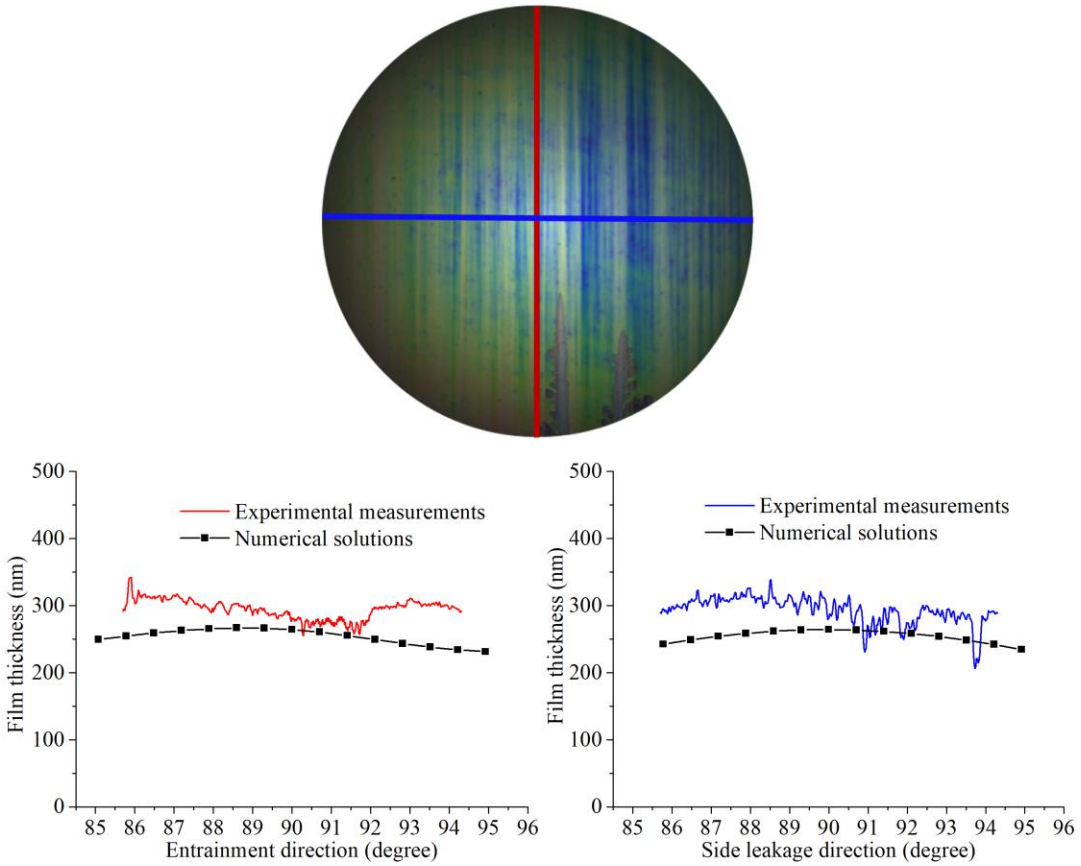
Experimental measurements
Numerical solutions
Film thickness (nm)
Entrainment direction (degree)
Side leakage direction (degree)

(a) 6.38s

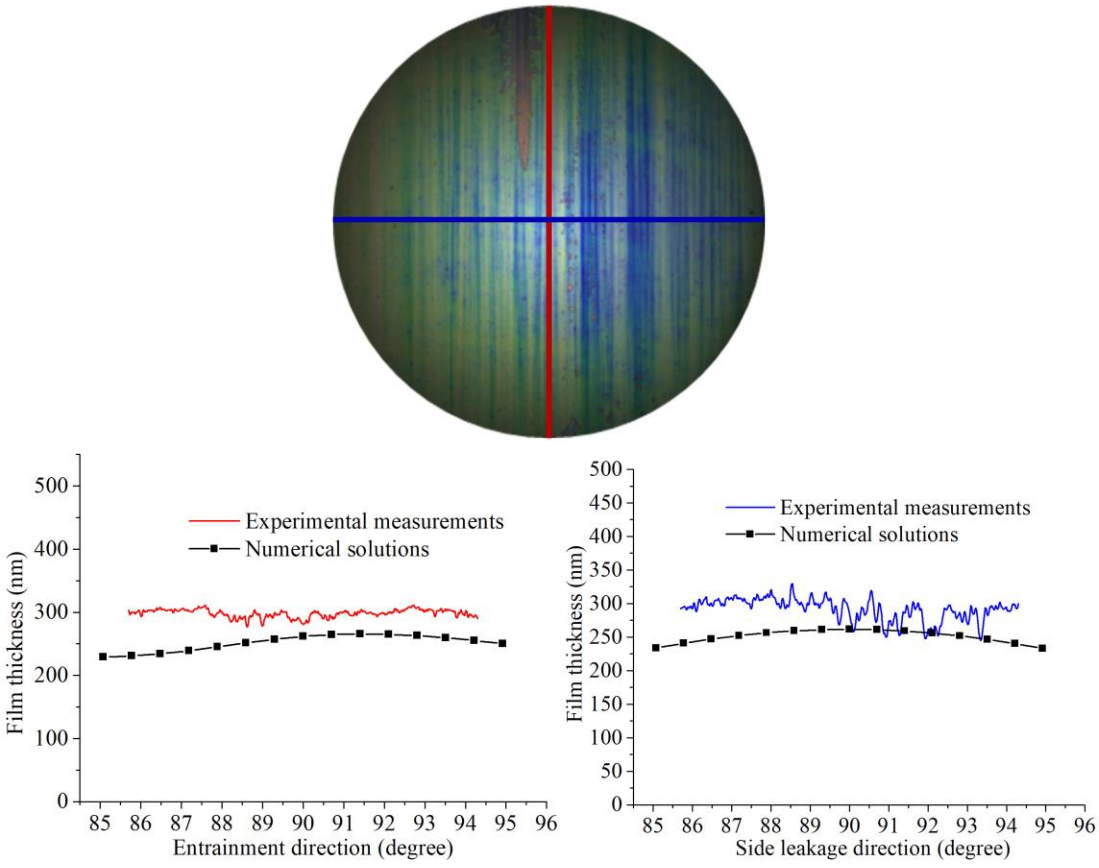
Experimental measurements
Numerical solutions
Film thickness (nm)
Entrainment direction (degree)
Side leakage direction (degree)

(b) 7.35s

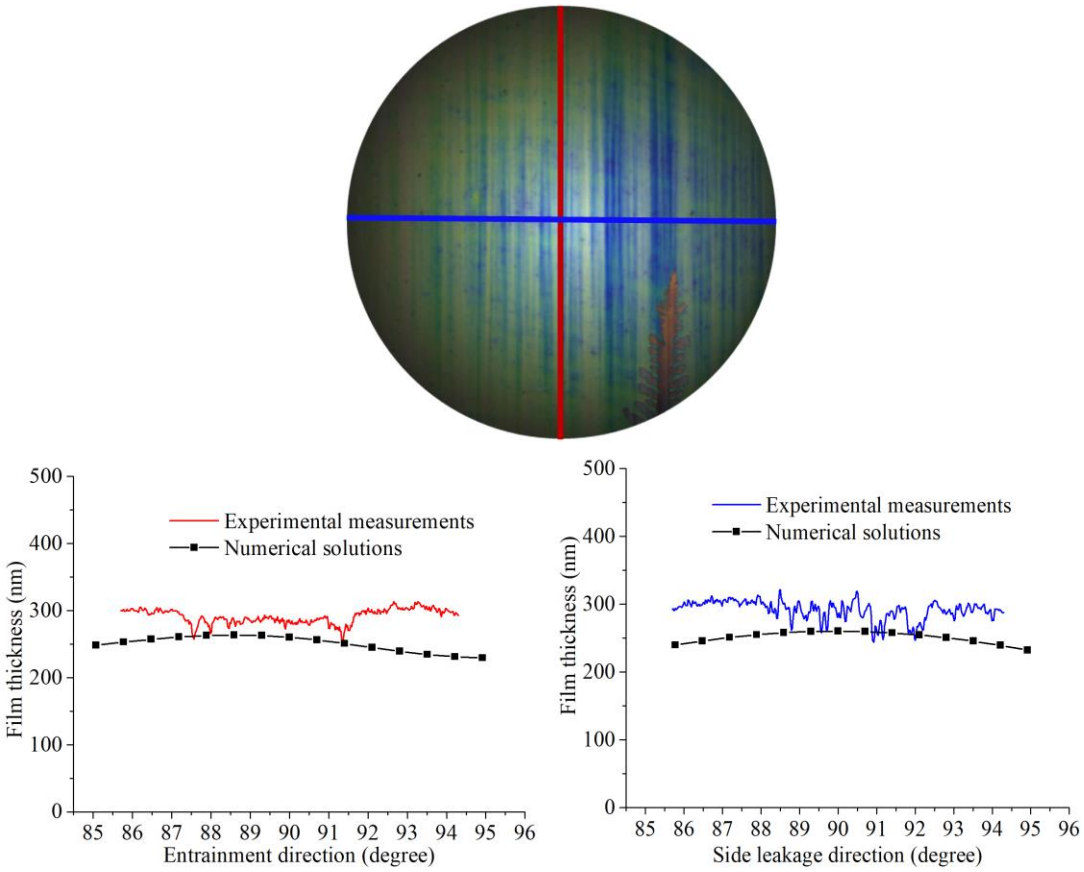

(c) 8.32s

Figure 6 The comparison of the cross-sectional film profiles in the entraining and side leakage directions between the experimental measurements and the numerical analyses at three time instants ((a) 6.38s, (b) 7.35 s, and (c) 8.32 s) for the SN100 mineral oil case.

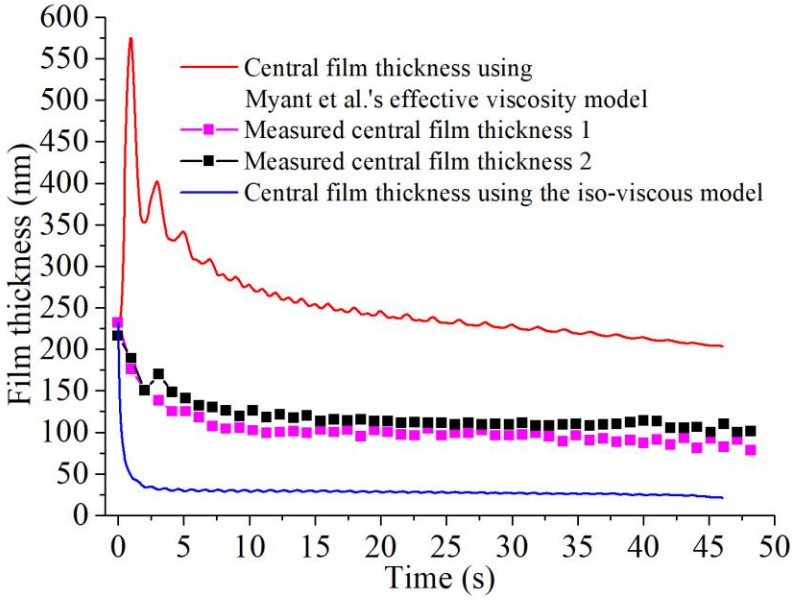

Figure 7 The comparisons between the experimentally measured and numerically calculated central film thicknesses at the equilibrium position of the pendulum. The central film thicknesses predicted by both the iso-viscous model and the effective viscosity model did not agree well with the experimental measurements for the 25% bovine serum solution case.

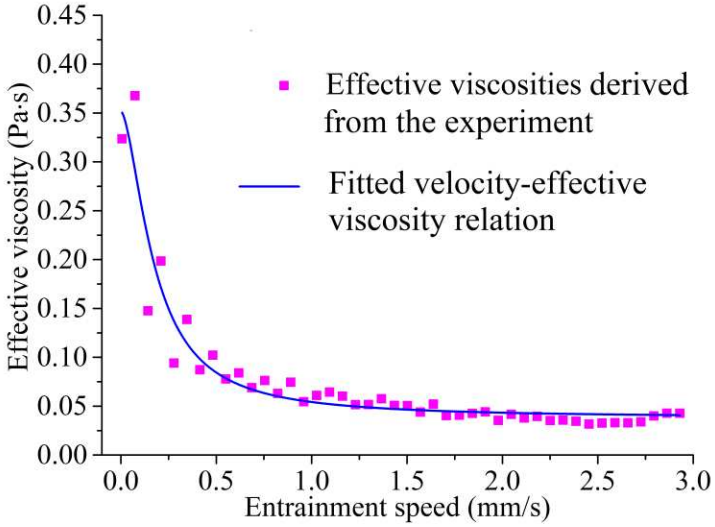

Figure 8 The effective viscosities derived from the film thicknesses measured by experiments and the full numerical solutions, and the fitted entrainment velocity-effective viscosity curve.

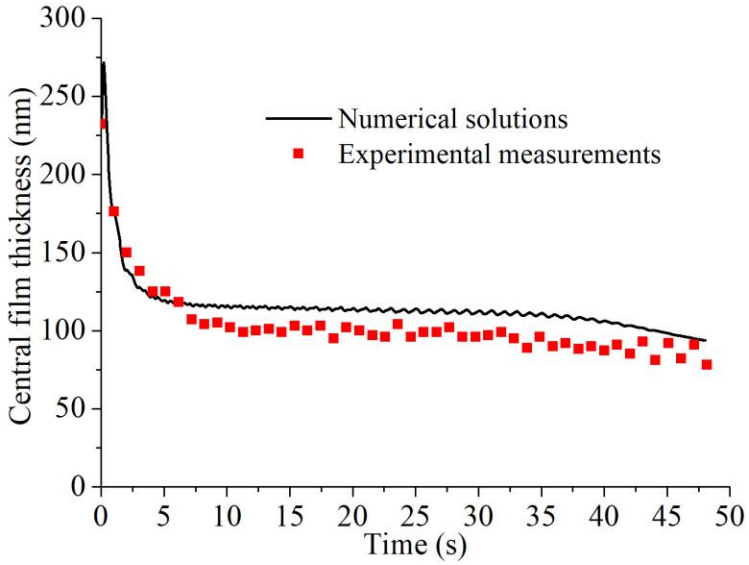

Figure 9 The comparison of the central film thickness between the experimental measurements and the numerical solutions solved using the new entrainment velocity-effective viscosity equation.

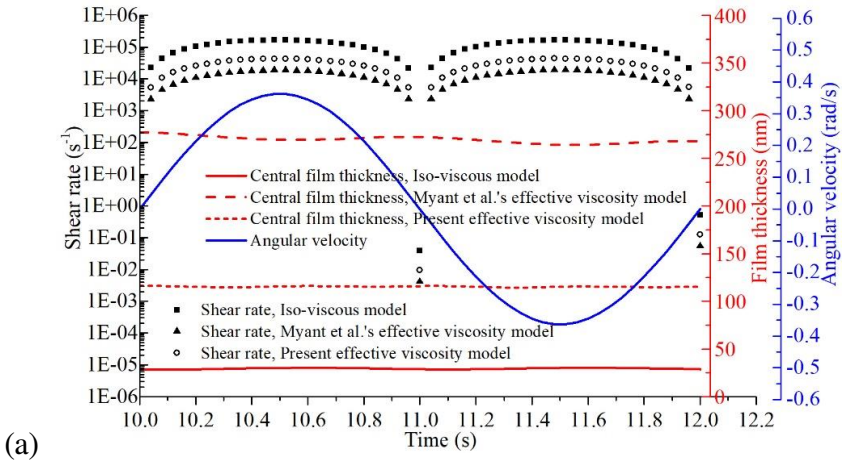

(a)

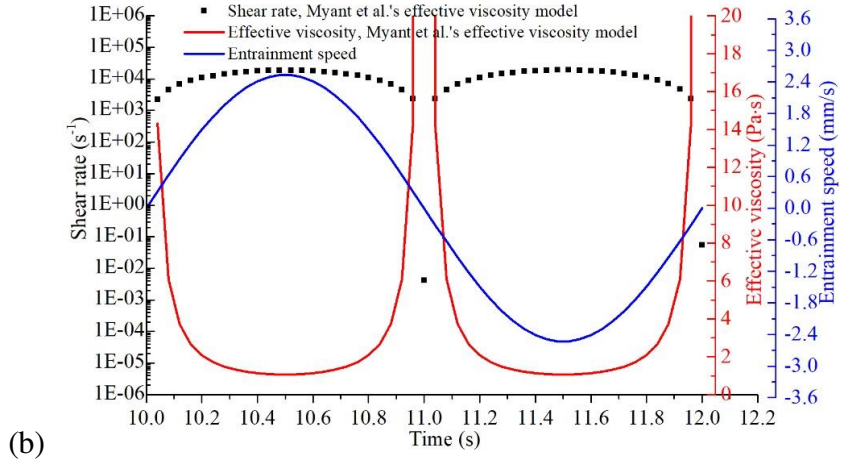

(b)

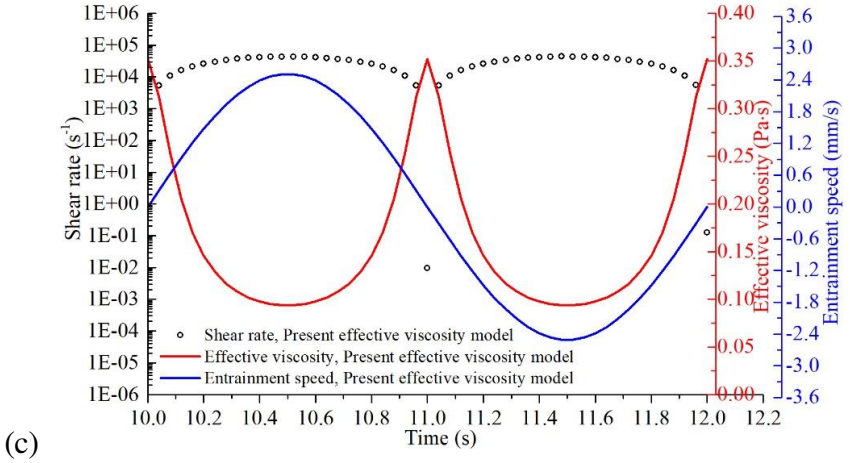

(c)

Figure 10 The variation in the central film thickness and shear rate of the three viscosity models (the iso-viscous, the effective viscosity model proposed by Myant et al., and the effective viscosity model proposed in this study) with the angular velocity within one oscillation cycle ((a)). The variations in the entraining velocity, the shear rate, and the effective viscosity within one cycle of the effective viscosity models proposed by Myant et al. and this study ((b) and (c), respectively).